FROM DECOUPLING TO ADAPTIVE TRANSFORMATION: A WIDER OPTIMIZATION SPACE FOR PTQ

Anonymous authors
Paper under double-blind review

ABSTRACT

Post-training low-bit quantization (PTQ) is useful to accelerate DNNs due to its high efficiency. Currently, finetuning through self-distillation feature reconstruction is one of the most effective PTQ techniques. However, when bitwidth goes to be extremely low, we find that current parameter update settings in PTQ feature reconstruction are sub-optimal. Considering all possible parameters and the ignored fact that integer weight can be obtained early before actual inference, we thoroughly explore 1) the setting of weight's quantization step into six cases by decoupling; 2) ignored learnable params in PTQ like BN and bias. Based on these explorations, we find there exist a wider optimization space and a better optimum. Considering these, we propose an Adaptive Quantization Transformation(AdaQTransform) for PTQ reconstruction, which provides adaptive per-channel transformation on the quant output feature, making them better fit FP32 counterpart and achieve lower PTQ feature reconstruction error. During inference, the AdaQTransform parameters can be merged without incurring additional inference costs. Based on AdaQTransform, for the first time, we build a general quantization setting paradigm subsuming current PTQs, QATs and other potential approaches. Experiments demonstrate that AdaQTransform expands the optimization space for PTQ and helps current PTQs find a better optimum over CNNs, ViTs, LLMs and low-level vision networks (image super-resolution). Specifically, AdaQTransform improves the current best PTQ by 5.7% on W2A2-MobileNet-v2. The code will be released.

1 INTRODUCTION

Low-bit model quantization (quant) generally consists of Quantization-Aware Training (QAT) and Post-Training Quantization (PTQ). PTQ requires a tiny amount of unlabeled data for calibration and does not demand the full training pipeline. Thus PTQ is always the first choice for fast model quantization. Traditional PTQ (Krishnamoorthi, 2018) searches quant parameters through Mean Squared Error(MSE). In 4 or 2 bits, these methods suffer from severe accuracy degradation. To improve low-bit PTQ, recent works propose quant-feature reconstruction through self-distillation, such as AdaRound (Nagel et al., 2020) / BRECQ (Li et al., 2021b) / NWQ (Wang et al., 2022).

Current PTQs evolve closer and closer towards QAT, except tiny unlabled calibration set and no need for training pipeline. The typical sign is that they optimize quant params with gradient descent by self-distillation. As shown in (a) and (b) of Figure.1, classic AdaRound-based PTQ process is as follows: (i) since PTQ owns no labeled dataset, the ground truth is the FP32 weight and FP32 activation; Conv's weight and bias are freezed; (ii) iteratively searches an optimal weight's quant-step s_w through the quant-error between FP32 weight and quantized weight, then freezes s_w and (iii) PTQ reconstruction: optimize weight's AdaRound parameter α and activation's quant-step s_x per layer/block/network through quant-error between FP32 and quant output activation.

Current PTQ SOTAs mostly adopt AdaRound for weight quantization. In order to make a stable up or down rounding learning, AdaRound adopts a frozen FP32 weight and a frozen weight's quant-step to ensure a fixed integer base. However, differing from that integer activation has to be computed online during inference, integer weight can be obtained early before inference, as described in Formula 4. With this ignored fact, still under a fixed integer weight, there exists a wider optimization space for the de-quantized FP32 weight, making it not limited to an ± 1 quant-step optimization distance, thus a lower reconstruction error might be met. That is, as shown in Formula 5, after computing

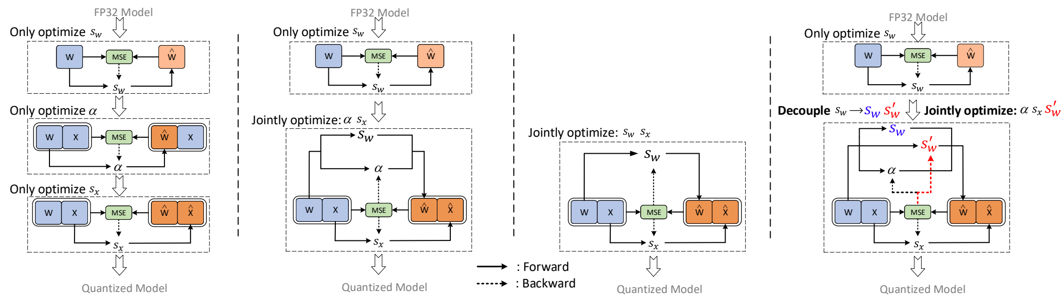

(a) Case 1.1.1: AdaRound and BRECQ (b) Case 1.1.2: QDROP and NWQ (c) Case 1.2: LSQ on PTQ (d) **Case 2.2: Ours on PTQ**

Figure 1: Different settings for weight's quant-step s_w. $W/X/\alpha/s_x$ denote weight/input/weight's adaround param/X's quant-step. Blue/orange box denote FP32/quantized values. The solid/dotted arrow line denote quantization forward/gradient backward process. s_{w} in (d) is decoupled as quant-step s_{w} and de-quant-step s'_{w}. Case 1.1.1 and others denote different quantization methods as Sec3.2.

the integer weight using s_w during fake quantization simulation (quant-process), the s_w used to convert integer weight into the FP32 counterpart (dequant-process) can be different. Or to say, the conventional weight's quant-step s_w can be decoupled apart as quant-step s_w and dequant-step s'_w according to different functions. With these operations, the adaround learning process is still stable since the adaround learning base, integer weight, is fixed. Nevertheless, can we obtain accuracy gain through decoupling? Now that PTQ evolves close to QAT, what will we gain if we directly optimize weight's quant-step into PTQ reconstruction like QAT as (c) of Figure.1? Considering all above, we thoroughly explore the setting of weight's quant-step into six possible cases through decoupling over various networks as Sec.3.2, where Case 1.1 is the current PTQ setting(AdaRound/BRECQ/NWQ), Case 1.2 is the current QAT's weight quant-step setting like LSQ (Esser et al., 2020) applied on PTQ reconstruction. We experimentally find a new setting Case 2.2, where we decouple quant-step, freeze integer weight and jointly optimize dequant-step as Formula 6, consistently performs the best.

At deeper optimization side, as Figure 2, Case 2.2 makes quant output better fit FP32 counterpart and achieves a wider optimization space. The decoupled de-quant step s'_w of weight finally achieves adaptive per-channel transformation on the output feature. Indeed, through visual and theoretical analysis, Case 2.2 equals to an adaptive per-channels linear transformation directly on output feature towards its FP32 counterpart as shown in Fig.2. Therefore, it is different from the common per-channel quant-step or offset like LSQ or LSQ+ (Bhalgat et al., 2020). Because current per-channel quant-step or offset does not change the distribution of output feature, which only optimizes the current input while ignores current PTQ's output feature reconstruction. In addition, current PTQs freeze Conv's bias away from PTQ reconstruction. We find out it is helpful to finetune bias b, which provides further translating on quant output to narrow quant-error gap.

Considering above and keep every setting as before, we introduce a scaling, ϵ, and a translating factor, η, into current quantization settings, namely **AdaQTranform**, to help better reconstruct quant output.

Although our AdaQTransform share some similarity on mathematics with normalization layer in network, it significantly differs from normalization as we shown in Sec.3.3.2. The normalization layer in PTQ can seen as a special form of AdaQTransform. AdaQTransform can be both helpful to networks/layers with normalization, e.g., high-level tasks like classification networks(ResNets(He et al., 2016)), or without normalization, e.g., low-level tasks like image super-resolution(EDSR (Lim et al., 2017)). In addition, based on AdaQTransform, we build a general unified paradigm subsuming quantization settings of current PTQs, QATs and our new decoupling case. The detailed expansions from the unified paradigm to specific quant-settings can be seen in Sec.3.3. Our contributions are:

- We fully explore weight's quant-step and other ignored parameters in PTQ. Based on the exploration, we propose AdaQTransform, which directly transforms the quant output towards the FP32 counterpart(ground truth), making a wider optimization space and a narrower quant-error gap.
- Based on AdaQTransform, for the first time, we build a general unified paradigm subsuming quantization parameter settings for current PTQs, QATs and other possible cases.
- We evaluate AdaQTransform across CNNs, ViTs, LLMs and image super-resolution network EDSR, which proves that AdaQTransform is orthogonal to current PTQs and consistently helps them to find a better optimum and achieve better PTQ performance without extra inference cost.

2 Related Work

Post Training Quantization (PTQ): As one of the best weight PTQ, AdaRound (Nagel et al., 2020) proposed an adaptive rounding for weight rather than rounding-to-nearest operation. BRECQ (Li et al., 2021a) found block-wise reconstruction behaves better than layer-wise ones. QDROP (Wei et al., 2022) explored how activation quantization affected weight tuning, and proposed a random activation quantization during weight adaround learning. NWQ (Wang et al., 2022) proposed a network-wise PTQ with inter-layer dependency. MRECG (Ma et al., 2023)/Bit-Shrink (Lin et al., 2023) tried to solve oscillation/sharpness problem. PD-Quant (Liu et al., 2023) proposed to consider global information based on prediction difference metric. PTQ4ViT (Yuan et al., 2022), APQ-ViT (Ding et al., 2022), and RepQ-ViT (Li et al., 2023) tried to solve the PTQ for Vision Transformer(ViT).

Differently, we find weight's quant-step can be safely decoupled, and experimentally find the best case for PTQ reconstruction among six possible cases. Based on this best case, we theoretically propose an AdaQTransform to provide adaptive per-channel linear transformation on output feature.

Training-Aware Quantization (QAT): Opposite to PTQ, QAT requires the whole FP32 training pipeline, including huge amounts of training data and the full FP32 training pipeline. Jacob et.al (Jacob et al., 2018b) proposed a fake quantizer simulation into QAT and to optimize by gradient descent with straight-through estimator (STE). PACT (Choi et al., 2018) proposed parameterized clipping activation to learn the quantization range. LSQ (Esser et al., 2020) proposed to learn the quantization step directly. LSQ+(Bhalgat et al., 2020) further proposed a learnable offset. Nagel (Nagel et al., 2022) tried to sovle oscillations in QAT. LSQ's learnable quant-step on PTQ is shown as (c) of Fig.1.

However, from Tab.1 Case 1.2, we find LSQ's(QAT) weight quant-step updating setting, where s_w is learnable and jointly optimized with s_x, is not the best for PTQ reconstruction. This is because PTQ owns only a tiny unlabeled calibration set thus it freezes FP32 weight as ground truth, totally different from QAT. Therefore, it is not suitable to directly borrow QAT's quant-step update setting into PTQ.

3 Method

3.1 Preliminaries and Current SOTA of PTQ

As current PTQ SOTAs, we perform per-channel weight quantization and per-layer activation quantization. A classic linear symmetric PTQ process is as Formula (1,2,3). s_w/s_x, $w_l/w_u/x_l/x_u$ is the quant-step, upper/lower bound of quantization levels of FP32 weight w and FP32 activation x. $\lfloor \frac{w}{s_w} \rceil$ / $\hat{w}$ are called quantized(integer) / de-quantized weight. $\lfloor \cdot \rceil / \lfloor \cdot \rfloor$ indicates rounding/floor operation. $h(\boldsymbol{\alpha})$ is AdaRound (Nagel et al., 2020) parameter of weight. $\sigma(\cdot)$ is Sigmoid function. They first initialize s_w through minimizing the MSE between FP32 and quantized weight as Formula (1). Then freezing s_w and optimizing AdaRound $h(\boldsymbol{\alpha})$ activation quantization as (2) through output feature reconstruction as (3). We can see FP32 weight w and FP32 bias b are freezed in current PTQs.

$$\hat{\boldsymbol{w}} = clip(\lfloor \frac{\boldsymbol{w}}{s_w} \rceil; w_l, w_u) \cdot s_w, \quad min_{\boldsymbol{s_w}} \ ||\hat{\boldsymbol{w}} - \boldsymbol{w}||_F^2 \tag{1}$$

$$\hat{\boldsymbol{w}} = clip(\lfloor \frac{\boldsymbol{w}}{s_w} \rfloor + h(\boldsymbol{\alpha}); w_l, w_u) \cdot s_w; \, h(\alpha) = clip(\sigma(\alpha) * 1.2 - 0.1, 0, 1); \, \hat{\boldsymbol{x}} = clip(\lfloor \frac{\boldsymbol{x}}{s_x} \rceil; x_l, x_u) \cdot s_x \tag{2}$$

$$\text{PTQ Reconstruction: } \hat{\boldsymbol{y}} = \hat{w} * \hat{x} + b = \sum((\lfloor \frac{\boldsymbol{w}}{\boldsymbol{s_w}} \rfloor + \boldsymbol{h(\alpha)}) \cdot s_w) * (\left[\frac{\boldsymbol{x}}{s_x}\right] \cdot s_x); \quad \min_{\boldsymbol{\alpha}, \boldsymbol{s_x}} ||\hat{\boldsymbol{y}} - \boldsymbol{y}||_F^2 \tag{3}$$

Fake and Real Quantization. In order to better optimize PTQ parameters through gradient descent, the quantization function is simulated in FP32 format, denoted as the '$Fake\ Quant$' bracket of Formula 4. During practical inference acceleration, the FP32 simulation is converted to be integer-arithmetic-only (Jacob et al., 2018a) as the '$Real\ Quant$' bracket of Formula (4).

$$\boldsymbol{y} \ = \ \underbrace{\sum \boldsymbol{w} * x + b}_{FP32} \ \approx \ \underbrace{\sum \hat{\boldsymbol{w}} * \hat{\boldsymbol{x}} + b}_{Fake\ Quant} \ = \ \underbrace{s \cdot \sum \boldsymbol{w_{int}} * \left[\frac{\boldsymbol{x}}{s_x}\right] + b}_{Real\ Quant} = \hat{y},$$
$$\text{where} \quad s = s_w \cdot s_x, \quad \boldsymbol{w_{int}} \ = \ clip(\lfloor \frac{\boldsymbol{w}}{s_w} \rfloor + h(\boldsymbol{\alpha}); w_l, w_u) \tag{4}$$

where $[\cdot]$ denotes rounding and clipping operations. $\boldsymbol{w_{int}}$ is integer weight, which can be obtained early before practical fixed-point inference as the lower part of Formula (4).

3.2 EMPIRICAL OBSERVATIONS: DECOUPLE QUANT-STEP OF WEIGHT

As the '$Real\ Quant$' of Formula 4, the $\boldsymbol{w_{int}}$ and $\boldsymbol{s_w}$ are determined before deployment, thus they can be treated as independent parameters. Given this property, for fake quantization, as Formula 5, we propose to decouple the quant-step of weight into quant-step s_w, which quantize FP32 weight to integer value, and dequant-step s'_w, which de-quantize integer weight back. Different from weight, quant-step of activation can not be decoupled since integer activation is different for different input.

$$\hat{\boldsymbol{w}} = clip(\lfloor \frac{\boldsymbol{w}}{s_w} \rfloor + h(\boldsymbol{\alpha}); w_l, w_u) \cdot s_w \quad \Rightarrow \quad \hat{\boldsymbol{w}} = clip(\lfloor \frac{w}{\boldsymbol{s_w}} \rfloor + h(\boldsymbol{\alpha}); w_l, w_u) \cdot s'_w \tag{5}$$

Under the condition where the quant-step of weight can be decoupled, for the first time, we fully explore different settings of weight's quant-step into six cases, based on whether quant-step is decoupled, and if decoupled, quant-step s_w and de-quant step s'_w are learnable or not after initialization.

- **Case 1**: the original single quant-step s_w is not decoupled as convention.
  - ⊙ **Case 1.1**: not participates joint PTQ reconstruction optimization, as (a) of Fig. 1.
    - ◊ Case 1.1.1: Weight PTQ and activation PTQ are seperated, like AdaRound/BRECQ.
    - ◊ Case 1.1.2: Consider Weight AdaRound into activation PTQ, like QDROP/NWQ.
  - ⊙ **Case 1.2**: participates joint optimization during feature reconstruction, as (b) of Fig.1.
    - ◊ current QAT methods, like LSQ. **QAT's updating setting is not the best for PTQ**.
- **Case 2**: the original single quant-step s_w is decoupled as two independent params s_w and s'_w.
  - ⊙ **Case 2.1**: Only quant-step s_w participates joint PTQ reconstruction optimization.
  - ⊙ **Case 2.2**: Only dequant-step s'_w participates PTQ reconstruction optimization, as(d) of Fig.1.
    - ⧫ frozen s_w: a fixed base for adaround learning; learnable s'_w: adaptive transformation.
  - ⊙ **Case 2.3**: s_w and s'_w both participate in joint PTQ reconstruction optimization.

To evaluate their efficiency, we conduct experiments on MobileNet-v2, ResNet-18, and MnasNet2.0.

Table 1: Acc@1 on ImageNet among different quant-step settings across various nets.

Methods	**W/A**	**MobileNet-v2**	**ResNet-18**	**MnasNet2.0**
Case 1.1.1 (AdaRound, last PTQ SOTAs)	3/2	0.32	41.65	1.07
Case 1.1.2 (NWQ, current PTQ SOTAs)	3/2	38.92	60.82	52.17
Case 1.2 (LSQ, QAT's SOTA on PTQ)	3/2	39.65	60.26	49.78
Case 2.1	3/2	38.77	59.90	48.40
Case 2.2	3/2	**42.60**	**61.06**	**54.19**
Case 2.3	3/2	41.42	60.86	49.33

We find out that Case 2.2, where we decouple the original quant-step s_w as s_w and s'_w then make only dequant-step s'_w learnablely participates joint PTQ reconstruction, shown as (d) of Fig 1, consistently provides the best performance, which even does a better job than Case 2.3. This is because (i) there is only a tiny unlabeled calibration set in PTQ, a frozen FP32 weight during finetuning makes the lowest quant-error. To further narrow quant-error gap, we need to apply AdaRound. and (ii) a stable AdaRound learning requires a fixed integer base but Case 2.1 and 2.3 bring fluid integer base.

Table 2: Visualization of Decoupling Case 2.2 during PTQ Reconstruction.

	0	5k	15k	20K		0	5k	15k	20K
s_{w1}	0.544	0.544	0.544	0.544	s_{w2}	0.943	0.943	0.943	0.943
s'_{w1}	0.544	0.508	0.444	0.442	s'_{w2}	0.943	0.902	0.796	0.795
Loss of Case 1.1.2	107	59.3	55.2	50.7	Loss of Case 2.2	107	**54.4**	**51.1**	**46.5**

We visualize the learning process of the dequant-step s'_w in Case 2.2 on W3A2 ResNet-18 as Tab. 2. At iteration 0, s_w and s'_w is decoupled from the the same value, then s_w is frozen and s'_w is learnable during PTQ reconstruction with weight's adaround param and activation quant-step. We can see Case 2.2's dequant-step s'_w is updated accordingly and provides lower loss than current PTQ Case 1.1.2.

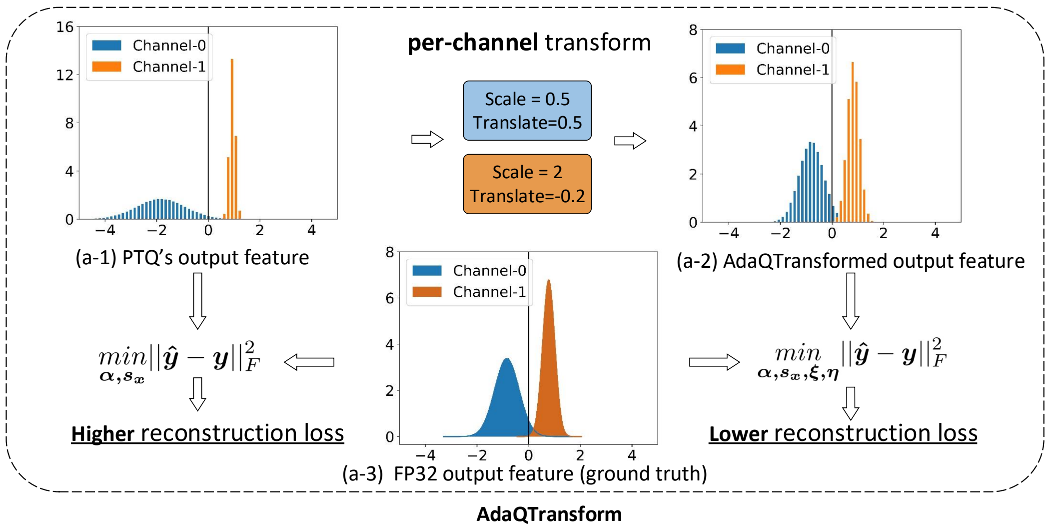

Figure 2: AdaQTransform: adaptive per-channel transformation on output feature.

3.3 From Decoupling to Adaptive Quant Transformation

Superficially, from empirical experiments in Sec.3.2, Case 2.2 consistently provides better accuracy and lower reconstruction loss. At deeper side, as Fig.2, Case 2.2 provides a better fit for each output channel to its FP32 ground truth. That is, Case 2.2 achieves adaptive per-channel scaling on the output feature. In theory, PTQ reconstruction in Formula.3 for Case 2.2 can be denoted as Formula.6, where $w_{floor} = \lfloor \frac{w}{s_w} \rfloor$ is frozen after initialization as Formula.1. Recall that We perform per-channel weight quantization and per-tensor activation quantization. Thus s'_w is a vector with out-channels elements while s_x is a scalar with one element. Therefore, the decoupled-out s'_w theoretically provides direct per-channel scaling on output feature to further minimize the quant-error gap.

$$\hat{\boldsymbol{y}} = \boldsymbol{s'_w} \cdot \left\{ s_x \cdot \sum (\boldsymbol{w_{floor}} + \boldsymbol{h}(\boldsymbol{\alpha})) * \left[\frac{\boldsymbol{x}}{s_x} \right] \right\} + b, \quad \text{objective: } \min_{\boldsymbol{\alpha}, \boldsymbol{s_x}, \boldsymbol{s'_w}} ||\hat{\boldsymbol{y}} - \boldsymbol{y}||_F^2 \tag{6}$$

A deeper look at Formula 6, there are two params, w_{floor} and b, left frozen. w_{floor} is frozen since a stable up or down rounding learning requires a fixed base. Bias b is frozen due to inherited PTQ tradition. However, as we know, current PTQ works step closer and closer towards QAT. We find out it is enough to finetune bias b with self-distillation between FP32 and quant output, which helps narrow the quantization error caused by quantized weight and quantized input, making their output fit closer to its FP32 counterpart, as shown in Fig.2. Therefore, in addition to per-channel scaling, our decoupling Case 2.2 can be further equipped with per-channel translating as

$$\hat{\boldsymbol{y}} = \boldsymbol{s'_w} \cdot \left\{ s_x \cdot \sum (\boldsymbol{w_{floor}} + \boldsymbol{h}(\boldsymbol{\alpha})) * \left[\frac{\boldsymbol{x}}{s_x} \right] \right\} + b', \quad \text{objective: } \min_{\boldsymbol{\alpha}, \boldsymbol{s_x}, \boldsymbol{s'_w}, \boldsymbol{b'}} ||\hat{\boldsymbol{y}} - \boldsymbol{y}||_F^2 \tag{7}$$

The PTQ reconstruction objective becomes the right of Formula 7. In order to be notation-consistent with previous methods as Formula 3, we introduce a per-channel scaling and translating factor, η, ξ, to denote Formula.7 as Formula.8, dubbed as **Ada**ptive **Q**uant **Transform**ation (**AdaQTransform**).

$$\hat{\boldsymbol{y}} = \boldsymbol{\xi} \cdot \left\{ \sum ((\lfloor \frac{\boldsymbol{w}}{\boldsymbol{s_w}} \rfloor + \boldsymbol{h}(\boldsymbol{\alpha})) \cdot s_w) * (\left[\frac{\boldsymbol{x}}{s_x} \right] \cdot s_x) \right\} + b + \boldsymbol{\eta}, \quad \text{objective: } \min_{\boldsymbol{\alpha}, \boldsymbol{s_x}, \boldsymbol{\xi}, \boldsymbol{\eta}} ||\hat{\boldsymbol{y}} - \boldsymbol{y}||_F^2 \tag{8}$$

3.3.1 No Extra Inference Cost in AdaQTransform

Although AdaQTransform add extra parameters to obtain finer-grained PTQ reconstruction, it cause no extra cost in actual inference as prior works like MRECG (Ma et al., 2023) and NWQ (Wang et al., 2022). After PTQ reconstruction is finished, the inference can be converted as Formula (9),

$$\hat{\boldsymbol{y}} = \widetilde{\boldsymbol{s}} \cdot \left\{ \sum (\boldsymbol{w_{int}} * \left[\frac{\boldsymbol{x}}{s_x} \right]) \right\} + \widetilde{b}, \quad \text{where } \widetilde{s} = \boldsymbol{\xi} \cdot \boldsymbol{s_w} \cdot \boldsymbol{s_x}, \ \widetilde{b} = b + \eta \tag{9}$$

3.3.2 Diffenrence between AdaQTransform and Normalization

Our AdaQTransform is significantly different from normalization, such as Batch/Group/Layer Normalizaion (BN/GN/LN), here we take BN as a example, in three points.

First, BN is used to stabilize FP32 model training while AdaQTransform is used to help quantized model better fit FP32 counterpart during self distillation. BN normalizes data with statistical mean and variance then accordingly scales and shifts them back. AdaQTransform directly learns a per-channel linear transformation from quantized feature to FP32 counterpart.

Second, current PTQ publications all fold BN into its proceeding Conv layer before quantization. Current QATs do not fold BN but they choose to update both statistical mean, variance and learnable scale, shift. As far as we know, there is no study exploring how BN influence PTQ up to now. For Conv-BN structures, if BN is not folded into its preceding Conv, and participates PTQ reconstruction, it achieves finer-grained per-channel transformation by making BN's per-channel scaling and translating parameter γ and β learnable as Formula (10) with frozen s_w and frozen mean μ and var σ^2. Compare Formula (10) with Formula (8), it can be seen as a special form of our AdaQTransform.

$$\hat{\boldsymbol{y}}=\frac{\boldsymbol{\gamma}}{\sqrt{\sigma^2+\epsilon}}\cdot\left\{\sum(\boldsymbol{w_{int}}\cdot\boldsymbol{s_w})*(\left[\frac{\boldsymbol{x}}{s_x}\right]\cdot\boldsymbol{s_x})\right\}+\boldsymbol{\beta}-\frac{\gamma\mu}{\sqrt{\sigma^2+\epsilon}}+b, \text{objective: } \min_{\boldsymbol{\alpha},\boldsymbol{s_x},\boldsymbol{\gamma},\boldsymbol{\beta}} ||\hat{\boldsymbol{y}}-\boldsymbol{y}||_F^2 \quad (10)$$

Thirdly, **AdaQTransform is both applicable to networks/layers with normalization or without normalization** like image super-resolution networks, e.g., EDSR (Lim et al., 2017), layers such as the latter Conv in Conv-BN-Conv, two Convs in Conv-(ReLU)-Conv, as demonstration in Sec.4

3.3.3 AdaQTransform is Orthogonal to Current Redistribution Methods

The core process of current redistribution methods for quantization, like LSQ+ (Bhalgat et al., 2020) with translating offset z_x or RepQ-ViT (Li et al., 2023) with the scaling vector $scale$, is as follows.

$$\text{LSQ+: } \hat{\boldsymbol{y}}=\hat{\boldsymbol{w}}*\hat{\boldsymbol{x}}+b=\sum(\lfloor\frac{\boldsymbol{w}}{\boldsymbol{s_w}}\rceil\cdot\boldsymbol{s_w})*(\left[\frac{\boldsymbol{x}-z_x}{s_x}\right]\cdot s_x+z_x)+b \quad (11)$$

$$\text{RepQ-ViT: } \hat{\boldsymbol{y}}=\hat{\boldsymbol{w}}*\hat{\boldsymbol{x}}+b=\sum(\lfloor\frac{\boldsymbol{w}\cdot\boldsymbol{scale}}{\boldsymbol{s_w}}\rceil\cdot\boldsymbol{s_w})*(\left[\frac{\boldsymbol{x}/\boldsymbol{scale}}{s_x}\right]\cdot s_x)+b \quad (12)$$

We can see their redistribution on output will be recovered. Thus they do no change the distribution of output feature. Differently, our AdaQTransform is directly performed on output feature and changes the distribution of output features, which further narrows the quant-error gap between y and $\hat{y}$,and is more suitable for PTQ's output feature reconstruction. Therefore, AdaQTransform is orthogonal to redistribution PTQs. Example for RepQ-ViT is as follows and experiments is as Tab.4

$$\hat{\boldsymbol{y}}=\xi\cdot\hat{\boldsymbol{w}}*\hat{\boldsymbol{x}}+b+\eta=\xi\cdot\sum((\lfloor\frac{\boldsymbol{w}\cdot\boldsymbol{scale}}{\boldsymbol{s_w}}\rfloor)\cdot\boldsymbol{s_w})*(\left[\frac{\boldsymbol{x}/\boldsymbol{scale}}{s_x}\right]\cdot s_x)+b+\eta \quad (13)$$

3.4 From AdaQTransform to General Quantization Paradigm

Formula 8 also builds a general quantization paradigm expressing quantization settings from current PTQs to current QATs and to our PTQ-suitable AdaQTransform. We can induct each one as follows,

- **From General Quant Paradigm to AdaRound/BRECQ**:
  $h(\alpha)$=AdaRound, $\xi=1,\eta=0$, objective: $\underset{\boldsymbol{s_w}}{min}||\hat{\boldsymbol{w}}-\boldsymbol{w}||_F^2, \underset{\boldsymbol{\alpha}}{min}||\hat{\boldsymbol{y}}-\boldsymbol{y}||_F^2$ then $\underset{\boldsymbol{s_x}}{min}||\hat{\boldsymbol{y}}-\boldsymbol{y}||_F^2$.
- **From General Quant Paradigm to QDROP/NWQ**:
  $h(\alpha)$=AdaRound, $\xi=1,\eta=0$, objective: $\underset{\boldsymbol{s_w}}{min}||\hat{\boldsymbol{w}}-\boldsymbol{w}||_F^2$ then $\underset{\boldsymbol{\alpha},\boldsymbol{s_x}}{min}||\hat{\boldsymbol{y}}-\boldsymbol{y}||_F^2$
- **From General Quant Paradigm to LSQ on PTQ**:
  $h(\alpha)=Round(\frac{\boldsymbol{w}}{\boldsymbol{s_w}}-\lfloor\frac{\boldsymbol{w}}{\boldsymbol{s_w}}\rfloor), \xi=1,\eta=0$, objective: $\underset{\boldsymbol{s_w},\boldsymbol{s_x}}{min}||\hat{\boldsymbol{y}}-\boldsymbol{y}||_F^2$.
- **From General Quant Paradigm to Our AdaQTransform**:
  $h(\alpha)$=AdaRound, ξ,η learnable, objective: $\underset{\boldsymbol{s_w}}{min}||\hat{\boldsymbol{w}}-\boldsymbol{w}||_F^2$ then $\underset{\boldsymbol{\alpha},\boldsymbol{s_x},\boldsymbol{\xi},\boldsymbol{\eta}}{min}||\hat{\boldsymbol{y}}-\boldsymbol{y}||_F^2$.
- **From General Quant Paradigm to QAT's LSQ**:
  $h(\alpha)=Round(\frac{\boldsymbol{w}}{\boldsymbol{s_w}}-\lfloor\frac{\boldsymbol{w}}{\boldsymbol{s_w}}\rfloor), \xi=1,\eta=0$, objective: $\underset{\boldsymbol{w},\boldsymbol{s_x},\boldsymbol{s_w},\boldsymbol{b}}{min} CrossEntropy(\hat{Logit}_{last}, label)$.

Algorithm 1: AdaQTransform PTQ

Input: Pretrained FP32 Model $\{W^l\}_{l=1}^N$; calib set;
Params : Activation's quant-step s_x; W's quant param: s_w, α. AdaQTranform: ξ, η

1_{st}: Iterative MSE Optimization for s_w as (1).

2_{nd}: PTQ Reconstruction.
for $j = 1$ to T iterations **do**
  for $i = 1$ to N layers **do**
    # Get output from FP32 and quantized
    $\hat{W}^i \xleftarrow{s_w, \alpha} W^i$ as Formula.2
    $\hat{x}^i \xleftarrow{s_x} x^i$ as Formula.2
    $y^i = W^i * x^i + b^i$;
    $\hat{y}^i = \xi \cdot \hat{W}^i * \hat{x}^i + b^i + \eta$; # as Formula.8
    $\Delta_i = ||y^i - \hat{y}^i||_F^2$
  $\Delta = \sum \Delta_i$, # Optimize s_x, α, ξ, η as (8)
Output: Quantized model

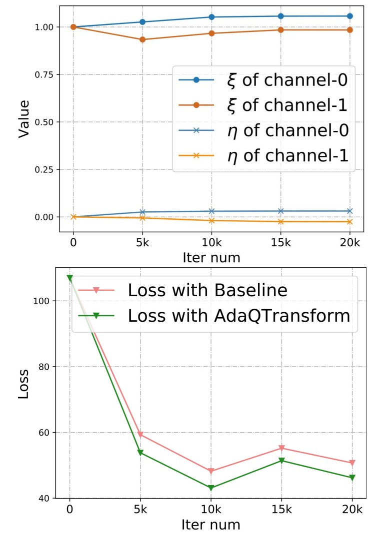

Figure 3: Visualization of AdaQTransform

4 EXPERIMENT

We evaluate AdaQTransform across various CNNs, ViTs, LLMs and image super-resolution networks using Pytorch (Paszke et al., 2019). Experimental settings are kept the same as each baselines. By convention, the first and last layer are quantized into 8 bits. AdaQTransform as Formula.8 is adopted. Integer inference with acceleration is performed with TVM on practical hardware.

4.1 EXPERIMENTS ON IMAGENET AND MS COCO

Table 3: Acc@1 on ImageNet among current PTQ methods.

Methods	W/A	Mobile-v2	Res-18	Reg-600	Mnas2.0
Full Prec.	32/32	72.49	71.08	73.71	76.68
AdaRound(Nagel et al., 2020)	4/4	64.33	69.36	-	-
AdaQuant(Hubara et al., 2021)	4/4	47.16	69.60	-	-
BRECQ(Li et al., 2021b)	4/4	66.57	69.60	68.33	73.56
QDROP(Wei et al., 2022)	4/4	68.84	69.62	71.18	73.71
PD-Quant (Liu et al., 2023)	4/4	68.33	69.30	71.04	73.30
MRECG (Ma et al., 2023)	4/4	68.84	69.46	71.22	-
NWQ (Wang et al., 2022)	4/4	69.14	69.85	71.92	74.60
AdaQTransform(ours)	**4/4**	**70.01**	**69.88**	**71.97**	**74.80**
BRECQ(Li et al., 2021b)	3/3	23.41	65.87	55.16	49.78
QDROP(Wei et al., 2022)	3/3	57.98	66.75	65.54	66.81
PD-Quant (Liu et al., 2023)	3/3	57.64	66.12	65.09	64.88
MRECG (Ma et al., 2023)	3/3	58.40	66.30	66.08	-
NWQ (Wang et al., 2022)	3/3	61.24	67.58	67.38	68.85
AdaQTransform(ours)	**3/3**	**63.44**	**67.73**	**67.81**	**69.52**
BRECQ(Li et al., 2021b)	2/2	0.24	42.54	3.58	0.61
QDROP(Wei et al., 2022)	2/2	13.05	54.72	41.47	28.77
PD-Quant (Liu et al., 2023)	2/2	13.67	53.14	40.92	28.03
MRECG (Ma et al., 2023)	2/2	14.44	54.46	43.67	-
NWQ (Wang et al., 2022)	2/2	26.42	59.14	48.49	41.17
AdaQTransform(ours)	**2/2**	**32.19**	**60.12**	**51.20**	**44.54**

We first experiment on ImageNet classification task over various CNNs and vision transformers as shown in Tab.(3,4). The calibration set consists of 1024 unlabeled images randomly selected from the training set. We adopt Adam optimizer, the same learning rate as (Wei et al., 2022; Ma et al., 2023) and 20k iterations for network-wise PTQ reconstruction as (Wang et al., 2022). The average experimental results over 5 runs are summarized in Tab.3. In W4A4, our method provides about 0-1% Acc@1 improvement compared to the strong baseline including NWQ (Wang et al., 2022), MRECG (Ma et al., 2023). In W3A3, our method improve MobileNet-v2 by 2.2% and MnasNet2.0 by 0.67%. In W2A2, where BRECQ shows nearly 0% Acc@1 on Mobile-v2 and Mnas2.0, our method still far outperforms NWQ by more than 3% on Mobile-v2, and Mnas2.0.

Table 4: Acc@1 on ImageNet for ViTs and DeiTs.

Methods	W/A	ViT-S	ViT-B	DeiT-S	DeiT-B
FP32	32/32	81.39	84.54	79.80	81.80
RepQ-ViT (Li et al., 2023)	6/6	80.43	83.62	78.90	81.27
AdaQTranform-RepQ-ViT	6/6	**80.59**	**83.89**	**79.12**	**81.53**
PTQ4ViT (Yuan et al., 2022)	4/4	42.57	30.69	34.08	64.39
APQ-ViT (Ding et al., 2022)	4/4	47.95	41.41	43.55	67.48
NWQ (Wang et al., 2022)	4/4	57.79	56.87	65.76	76.06
AdaQTransform-NWQ	4/4	**58.12**	**57.24**	**66.34**	**76.20**
RepQ-ViT (Li et al., 2023)	4/4	65.05	68.48	69.03	75.61
AdaQTranform-RepQ-ViT	4/4	**70.40**	**76.47**	**73.50**	**78.93**

For vision transformers, we experiments on ViT (Dosovitskiy et al., 2021) and DeiT (Touvron et al., 2021) as Tab.4. Our AdaQTransform outperforms NWQ by 0.5%, and outperforms PTQ4ViT (Yuan et al., 2022) and APQ-ViT (Ding et al., 2022) by a large margin, about 10%-32% better. Then we apply AdaQTranform into RepQ-ViT. We can see AdaQTransform helps RepQ-ViT improve about 4% in W4A4 and 0.3% in W6A6. Thus it demonstrates AdaQTranform helps narrow the quant-error gap between the quantized and FP32 activation.

Table 5: mAP on MS COCO for object detection.

Methods	W/A	Faster RCNN		RetinaNet	
		ResNet-50	ResNet-18	ResNet-50	MobileNet-v2
FP32	32/32	40.26	34.91	37.39	33.31
BRECQ (Li et al., 2021a)	4/4	37.19	33.41	34.67	29.81
QDROP (Wei et al., 2022)	4/4	38.53	33.57	35.81	31.47
NWQ (Wang et al., 2022)	4/4	38.54	33.63	35.98	31.81
AdaQTransform(ours)	4/4	**38.62**	**33.87**	**35.96**	**31.93**
QDROP (Wei et al., 2022)	3/3	33.49	31.21	32.13	27.55
NWQ (Wang et al., 2022)	3/3	35.25	31.88	32.45	28.43
AdaQTransform(ours)	3/3	**35.72**	**32.25**	**32.48**	**28.86**
QDROP (Wei et al., 2022)	2/2	21.05	21.95	20.27	12.01
NWQ (Wang et al., 2022)	2/2	25.01	23.92	22.95	16.21
AdaQTransform(ours)	2/2	**27.79**	**26.10**	**24.13**	**18.10**

For object detection, we experiments on one-stage RetinaNet (Lin et al., 2017) and two-stage Faster RCNN (Ren et al., 2015), where Res-18, Res-50 and Mobile-v2 are selected as backbones respectively. As (Wei et al., 2022; Li et al., 2021b), we quantize the input and output layers of the network to 8 bits, do not quantize the head of the detection model, and quantize the neck (FPN). Results are shown in Tab.5. In W3A3 setting, AdaQTransform improves the mAP of Res-50-based Faster RCNN by 0.5% and Mobile-v2-based RetinaNet by 0.4%. In harder W2A2 setting, AdaQTransform achieves about 1% mAP improvement over the current best method across all four experimental networks, which obtains a 2.78% improvement on Res-50-based Faster RCNN.

4.2 EXPERIMENTS ON IMAGE SUPER-RESOLUTION. (NETWORKS WITHOUT NORMALIZATION)

As shown on Sec. 3.3.2, layer normalization can be seen as a special form of our AdaQTransform. To show the effectiveness of AdaQTransform on networks without layer normalization, we experiment on image super-resolution networks, i.e., EDSR of scale 4 (Lim et al., 2017). We borrow base code from AdaBM (Hong & Lee, 2024) and follow all the same settings except that we apply our AdaQTransform to AdaBM. The calibration dataset, 100 LR images, is randomly sampled from the DIV2K (Timofte et al., 2017) training dataset. The quantization range for activation is initialized using MinMax and quantization step for weight is initialized by OMSE. Then we freeze the network weights and finetune the quantization parameters for 10 epochs using Adam optimizer. For evaluation metrics, we measure reconstruction accuracy using the peak signal-to-noise ratio (PSNR) and the structural similarity index (SSIM) on Set5/Set14/Urban100/BSD100 (Huang et al., 2015). To compare the computational complexity of the quantized network, we report the feature average bit-width (FAB) that is averaged throughout the images of the test dataset.

As shown in Tab. 6, where AdaQTrans† denotes we apply our AdaQTransform to AdaBM (Hong & Lee, 2024), we can see our AdaQTransform consistently helps AdaBM improve the PSNR and SSIM on 4 experimental test sets and 4/3/2-bit quantization settings. Tab. 6 demonstrates our AdaQTransform differs from layer normalization and gains from a wider optimization space: it helps the quant output feature better fit the FP32 counterpart and achieves lower PTQ quantization error.

Table 6: PTQ for EDSR of scale 4.

Model	W/A	Set5		Set14		BSD100		Urban100	
		FAB	PSNR/SSIM	FAB	PSNR/SSIM	FAB	PSNR/SSIM	FAB	PSNR/SSIM
EDSR (X4)	32/32	32	32.10 / 0.893	32	28.57 / 0.781	32	27.56 / 0.736	32	26.02/ 0.784
AdaBM-paper	4/4MP	3.8	31.02 / 0.860	3.7	27.87 / 0.751	3.5	26.91 / 0.700	3.7	25.11 / 0.736
AdaQTrans†	4/4MP	**3.7**	**31.17 / 0.870**	**3.5**	**27.99 / 0.761**	**3.5**	**27.04 / 0.713**	**3.7**	25.03 /**0.742**
AdaBM	4/4	4	29.42 / 0.821	4	26.81 / 0.724	4	26.44 / 0.687	4	23.87 / 0.685
AdaQTrans†	4/4	**4**	**31.41 / 0.845**	**4**	**27.55 / 0.742**	**4**	**26.81 / 0.698**	**4**	**24.64 / 0.718**
AdaBM	3/3	3	28.93 / 0.804	3	26.49 / 0.711	3	26.24 / 0.679	3	23.53 / 0.667
AdaQTrans†	3/3	**3**	**29.01 / 0.810**	**3**	**26.55 / 0.716**	**3**	**26.27 / 0.683**	**3**	**23.56 / 0.672**
AdaBM	2/2	2	28.76 / 0.791	2	26.38 / 0.702	2	26.17 / 0.673	2	23.45 / 0.657
AdaQTrans†	2/2	**2**	**28.84 / 0.802**	**2**	**26.44 / 0.712**	**2**	**26.23 / 0.681**	**2**	**23.46 / 0.666**

As shown in Fig.4, our AdaQTransform helps AdaBM produces visually better reconstructed images with more details, e.g., AdaBM is relatively slur on the arch curve while AdaQTransform is clearer.

GT(img014) AdaBM AdaQTransform

Figure 4: Qualitative results on Urban100 with 4-bit EDSR-based models.

Table 7: AdaQTransform for LLMs on LAMADA.

Method	W/A	Opt-1.3B	Opt-6.7B
FP32	32/32	72.0%	79.8%
Naive	8/8	69.1%	41.9%
SmoothQuant (Xiao et al., 2023)	8/8	70.8%	80.0%
AdaQTransform†	8/8	**71.2%**	**80.1%**
SmoothQuant	6/6	66.2%	75.4%
AdaQTransform†	6/6	**67.5%**	**75.6%**

Table 8: Exploration for BN and AdaQTransform

Methods	W/A	Mobile-v2	Res-18	Reg-600
NWQ(BN-Floded)	3/3	61.24	67.58	67.38
BN-Not-Folded	3/3	63.26	67.67	67.65
Decoupling	3/3	63.17	67.64	67.42
AdaQTransform	3/3	**63.44**	**67.73**	**67.81**
NWQ(BN-Floded)	2/2	26.42	59.14	48.49
BN-Not-Folded	2/2	32.09	60.09	51.18
Decoupling	2/2	31.43	59.91	50.32
AdaQTransform	2/2	**32.19**	**60.12**	**51.20**

4.3 Experiments on Large Language Models (LLM)

As Tab.7, we appaly our AdaQTransform to SmoothQuant (Xiao et al., 2023), denoted as AdaQTransform†, on LLM models Opt-1.3B and Opt-6.7B. We can see our AdaQTransform can help SmoothQuant to further improve performance, especially in W6A6, about 1.3% gain on Opt-1.3B.

4.4 Ablation Study on ImageNet

4.4.1) **AdaQTransform V.s. BN**: For networks with normalization(BN/GN/LN), as we know, there have not been an academic PTQ work exploring BN's folding or not. Thus we explore it as Tab.8 based on NWQ which adopts BN-Folded setting by default. For BN-Not-Folded, we jointly optimize BN's learnable params γ and β. It provides almost the same accuracy whether to update BN's statistical params μ, σ or not. We see BN-Not-Folded provides better performance than BN-Folded (NWQ). AdaQTransform provides tiny better accuracy than BN-Not-Folded, since AdaQTransform can be applied on layers with BN (equals to BN-Not-Folded) and other layers without BN. Therefore, as Sec.3.3.2, **AdaQTransform subsumes BN-Not-Folded, and covers a wider application range**.

4.4.2) **Visualization for AdaQTransform**: As Fig.3.4, AdaQTransform achieves adaptive per-channel transformation with adaptive ξ, η for different output channels during PTQ reconstruction, and converges to a lower loss than baseline methods.

4.5 Inference Cost Comparison

We perform pure 4-bit/8-bit integer inference with TVM on hardware. The inference source code is borrowed from HAWQ (Yao et al., 2021). As convention, the first and last layer is in 8 bits. The middle layer convolution is 4bits. Input is 8-bit integers with shape (8, 3, 224, 224). The average inference time per sample over 30 measurement, each with 50 inference, is as follows. AdaQTranform improves accuracy without extra inference cost.

Table 9: W4A4 integer inference cost with TVM on hardware

Net	Acc@1	Time	params	Prams*Bit	FLOPs*Bit
Mobile-V2-NWQ (Wang et al., 2022)	69.14%	0.16 ms	3.51 M	20.79 M	6.36 G
Mobile-V2-AdaQTransform	**70.01%**	0.16 ms	3.51 M	20.79 M	6.36 G

5 Conclusion

In this paper, we propose a novel PTQ approach called AdaQTransform, based on full exploration on weight's quantization step through Decoupling over various networks and bitwidths. AdaQTransform provides adaptive per-channel transformation on the output feature produced from per-tensor quantized input activation, thus helps quant output better fit FP32 feature and achieves lower PTQ feature reconstruction error. The extra AdaQTransform params can be merged during inference thus without extra inference cost. For the first time, AdaQTransform builds a general paradigm in quantization parameter update settings from current PTQs to QATs. Experiments on CNNs, ViTs, LLMs, and image super-resolution networks demonstrate AdaQTransform sets up a new PTQ SOTA.

REFERENCES

Yash Bhalgat, Jinwon Lee, Markus Nagel, Tijmen Blankevoort, and Nojun Kwak. Lsq+: Improving low-bit quantization through learnable offsets and better initialization. In *CVPRW*, June 2020.

Jungwook Choi, Zhuo Wang, Swagath Venkataramani, Pierce I-Jen Chuang, Vijayalakshmi Srinivasan, and Kailash Gopalakrishnan. Pact: Parameterized clipping activation for quantized neural networks. *CoRR*, 2018.

Yifu Ding, Haotong Qin, Qinghua Yan, Zhenhua Chai, Junjie Liu, Xiaolin Wei, and Xianglong Liu. Towards accurate post-training quantization for vision transformer. In *ACM-MM*, pp. 5380–5388. ACM, 2022.

Alexey Dosovitskiy, Lucas Beyer, Alexander Kolesnikov, Dirk Weissenborn, Xiaohua Zhai, Thomas Unterthiner, Mostafa Dehghani, Matthias Minderer, Georg Heigold, Sylvain Gelly, Jakob Uszkoreit, and Neil Houlsby. An image is worth 16x16 words: Transformers for image recognition at scale. *ICLR*, 2021.

Steven K. Esser, Jeffrey L. McKinstry, Deepika Bablani, Rathinakumar Appuswamy, and Dharmendra S. Modha. Learned step size quantization. In *ICLR*. OpenReview.net, 2020.

Kaiming He, Xiangyu Zhang, Shaoqing Ren, and Jian Sun. Deep residual learning for image recognition. In *CVPR*, pp. 770–778, 2016.

Cheeun Hong and Kyoung Mu Lee. Adabm: On-the-fly adaptive bit mapping for image super-resolution. In *CVPR*, pp. 2641–2650, June 2024.

Jia-Bin Huang, Abhishek Singh, and Narendra Ahuja. Single image super-resolution from transformed self-exemplars. In *CVPR*, pp. 5197–5206, 2015.

Itay Hubara, Yury Nahshan, Yair Hanani, Ron Banner, and Daniel Soudry. Accurate post training quantization with small calibration sets. In *ICML*, pp. 4466–4475, 2021.

Benoit Jacob, Skirmantas Kligys, Bo Chen, and Menglong Zhu. Quantization and training of neural networks for efficient integer-arithmetic-only inference. In *CVPR*, 2018a.

Benoit Jacob, Skirmantas Kligys, Bo Chen, Menglong Zhu, Matthew Tang, Andrew Howard, Hartwig Adam, and Dmitry Kalenichenko. Quantization and training of neural networks for efficient integer-arithmetic-only inference. In *CVPR*, 2018b.

Raghuraman Krishnamoorthi. Raghuraman krishnamoorthi. quantizing deep convolutional networks for efficient inference: A whitepaper. *arXiv preprint arXiv:1806.08342*, 2018.

Yuhang Li, Ruihao Gong, Xu Tan, Yang Yang, Peng Hu, Qi Zhang, Fengwei Yu, Wei Wang, and Shi Gu. Brecq: Pushing the limit of post-training quantization by block reconstruction. *ICLR*, 2021a.

Yuhang Li, Ruihao Gong, Xu Tan, Yang Yang, Peng Hu, Qi Zhang, Fengwei Yu, Wei Wang, and Shi Gu. Brecq: Pushing the limit of post-training quantization by block reconstruction. *arXiv preprint arXiv:2102.05426*, 2021b.

Zhikai Li, Junrui Xiao, Lianwei Yang, and Qingyi Gu. Repq-vit: Scale reparameterization for post-training quantization of vision transformers. In *ICCV*, pp. 17227–17236, 2023.

Bee Lim, Sanghyun Son, Heewon Kim, Seungjun Nah, and Kyoung Mu Lee. Enhanced deep residual networks for single image super-resolution. In *CVPRW*, July 2017.

Chen Lin, Bo Peng, Zheyang Li, Wenming Tan, Ye Ren, Jun Xiao, and Shiliang Pu. Bit-shrinking: Limiting instantaneous sharpness for improving post-training quantization. In *CVPR*, pp. 16196–16205, June 2023.

Tsung-Yi Lin, Priya Goyal, Ross B. Girshick, Kaiming He, and Piotr Dollár. Focal loss for dense object detection. In *ICCV*, pp. 2999–3007, 2017.

Jiawei Liu, Lin Niu, Zhihang Yuan, Dawei Yang, Xinggang Wang, and Wenyu Liu. Pd-quant: Post-training quantization based on prediction difference metric. In *CVPR*, pp. 24427–24437, June 2023.

Yuexiao Ma, Huixia Li, Xiawu Zheng, Xuefeng Xiao, Rui Wang, Shilei Wen, Xin Pan, Fei Chao, and Rongrong Ji. Solving oscillation problem in post-training quantization through a theoretical perspective. In *CVPR*, pp. 7950–7959, June 2023.

Markus Nagel, Rana Ali Amjad, Mart van Baalen, Christos Louizos, and Tijmen Blankevoort. Up or down? adaptive rounding for post-training quantization. In *ICML*, volume 119, pp. 7197–7206, 2020.

Markus Nagel, Marios Fournarakis, Yelysei Bondarenko, and Tijmen Blankevoort. Overcoming oscillations in quantization-aware training. In *ICML*, 2022.

Adam Paszke, Sam Gross, Francisco Massa, Adam Lerer, James Bradbury, Gregory Chanan, Trevor Killeen, Zeming Lin, Natalia Gimelshein, Luca Antiga, et al. Pytorch: An imperative style, high-performance deep learning library. In *NeurIPS*, 2019.

Shaoqing Ren, Kaiming He, Ross Girshick, and Jian Sun. Faster r-cnn: Towards real-time object detection with region proposal networks. *NeurIPS*, 28, 2015.

Radu Timofte, Eirikur Agustsson, and et.al. Ntire 2017 challenge on single image super-resolution: Methods and results. *CVPRW*, pp. 1110–1121, 2017. URL https://api.semanticscholar.org/CorpusID:484327.

Hugo Touvron, Matthieu Cord, Matthijs Douze, Francisco Massa, Alexandre Sablayrolles, and Herve Jegou. Training data-efficient image transformers amp; distillation through attention. In *ICML*, 2021.

Changbao Wang, Dandan Zheng, Yuanliu Liu, and Liang Li. Leveraging inter-layer dependency for post -training quantization. In *NeurIPS*, 2022.

Xiuying Wei, Ruihao Gong, Yuhang Li, Xianglong Liu, and Fengwei Yu. Qdrop: Randomly dropping quantization for extremely low-bit post-training quantization. In *ICLR*, 2022.

Guangxuan Xiao, Ji Lin, Mickael Seznec, Hao Wu, Julien Demouth, and Song Han. SmoothQuant: Accurate and efficient post-training quantization for large language models. In *ICML*, 2023.

Zhewei Yao, Zhen Dong, Zhangcheng Zheng, Amir Gholami, Jiali Yu, Eric Tan, Leyuan Wang, Qijing Huang, Yida Wang, Michael W. Mahoney, and Kurt Keutzer. Hawqv3: Dyadic neural network quantization. *ICML*, 2021.

Zhihang Yuan, Chenhao Xue, Yiqi Chen, Qiang Wu, and Guangyu Sun. Ptq4vit: Post-training quantization for vision transformers with twin uniform quantization. In *ECCV*, volume 13672, pp. 191–207. Springer, 2022.